ASTRONOMY & ASTROPHYSICS
SUPPLEMENT SERIES

Astron. Astrophys. Suppl. Ser. **121,** 553-568 (1997)

Correction of the "piston effect" in optical astronomical interferometry

I. Modulus and phase gradient of the visibility function restoration

G. Perrin[1]

Observatoire de Paris, DESPA, 5 place Jules Janssen, F-92195 Meudon, France

Received November 13, 1995; accepted November 7, 1996

Abstract. An a posteriori method to cancel out atmospheric optical path fluctuations to achieve accurate phase restoration and spectral analysis of interferograms is presented in this paper. The correction algorithm is based on classical noise reduction methods. The consequence of piston noise is twofold: 1) loss of spectral information; 2) loss of visibility phase. A method to measure the modulus and the phase gradient of visibilities is explained and examples of restoration of simulated spectra and visibilities for various S/N ratios are presented.

Key words: atmospheric effects — methods: data analysis — technics: interferometric

1. Introduction

Visible and infrared interferometry is one of the most promising technics in the coming years to achieve high resolution imaging in astrophysics. The equivalent technique in radio wavelengths is providing the astrophysical community with sharp images impossible to obtain with classical single antennas due to fundamental diffraction limitations. At optical wavelengths, coherence of light measurements are strongly degraded by atmospheric turbulence and may even become impossible. A partial correction of turbulence modes can be achieved and is already producing interesting results for imaging. Nevertheless, adaptive optics cannot compensate for the 0-order mode of atmospheric distortion of wavefronts (the optical path fluctuations or "piston effect") which causes the loss of phase[1] information in interferometry cancelling any attempt to reconstruct high resolution images. White fringe position servoing systems (fringe trackers) make up for the optical path fluctuations in real time and lock the system onto the white fringe to perform low noise acquisition through long integration time, but they fail to record a long sequence containing spectral information. The paper starts with a presentation (Sect. 2) of interferometry and more especially Double Fourier interferometry and explains why optical path fluctuations effects are undesirable in interferometry. In Sect. 3 the properties of atmospheric optical path fluctuations are listed and simulations are presented. The piston correction method is explained in Sect. 4 and results on simulated interferograms are presented. Section 5 is the analysis of the results.

Send offprint requests to: G. Perrin (perrin@hplyot.obspm.fr)

[1] The position of the white light fringe measured in opd in wide-band interferometry is roughly, to within a $\frac{\lambda}{2\pi}$ factor, the phase of the image Fourier transform, i.e. the phase of the complex visibility.

2. General context

The aim of this section is essentially to provide the reader with a few classical notations as well as basic concepts of interferometry. Paragraph 2.1 is a brief theoretical tutorial on inteferometry. The purpose of the Double Fourier interferometric mode probing both temporal and spatial coherence properties of sources is explained in paragraph 2.2. Eventually, paragraph 2.3 adresses the aim of this paper, that is to say the nature of the disturbances generating optical path fluctuations.

2.1. Brief tutorial on interferometry

Equations derivations are classical and can be found in litterature (Goodman 1985 for example). Nevertheless, I intend to give a fundamental subset of equations whose accurate knowledge is mandatory for a good understanding of the remaining of the article. Let us consider two pupils P_1 and P_2 of an interferometer and the corresponding sampled complex amplitudes of an astronomical wavefront $A_1(\sigma, t)$ and $A_2(\sigma, t)$, where σ is the wavenumber and t is time. The two amplitudes are combined and sent to a detector. The monochromatic energy detected at the

output of the combiner is proportional to the average squared modulus (on a time scale far greater than the period of the wave) of the sum of the two fields:

$$I(\sigma,t) = < |A_1(\sigma,t) + A_2(\sigma,t)|^2 >_t . \quad (1)$$

For sake of simplicity, all multiplicative coefficients (detector gain, interferometer transmission, etc ...) will be set to one and their expressions will be dropped in the following equations. The monochromatic energy collected by the two pupils (which is proportionnal to the spectrum of the source) is supposed to be the same and the normalized total energy over the bandwidth is noted $B(\sigma)$. Equation (1) is then rewritten as:

$$\begin{aligned} I(\sigma,t) &= B(\sigma) + 2 < A_1(\sigma,t)\, A_2^*(\sigma,t) >_t \\ &= B(\sigma) + B(\sigma)\, Re\left\{\gamma_{12}(\sigma,t)\right\}, \end{aligned} \quad (2)$$

where $\gamma_{12}(\sigma,t)$ is the complex degree of coherence of the two beams coming from the source and collected by the two pupils of the interferometer. For a monochromatic radiation, it has a simple expression as a function of the delay τ between the two beams (Goodman 1985):

$$\gamma_{12}(\sigma,t) = V_{12}(\sigma)\mathrm{e}^{-2j\pi\sigma v t}, \quad (3)$$

where v is the rate of change of opd. V_{12} is the coherence factor of the two beams or fringe visibility and is wavelength dependent. The value of visibility is determined by the geometrical aspect of the source and by the geometrical characteristics of the baseline. It is the Fourier transform of the intensity distribution of the source at a spatial frequency equal to the vector baseline over wavelength according to the Van Cittert-Zernike theorem (Born & Wolf 1980; Goodman 1985). Visibility[2] is the observable measured by interferometers.

It is equivalent to express delay either as a temporal delay τ or as an optical path difference x as the ratio of the two is the speed of the fringes v. In wide band, Eq. (2) becomes:

$$I(x) = 1 + Re\left\{\int_{\mathrm{band}} B(\sigma)V_{12}(\sigma)\mathrm{e}^{-2j\pi\sigma x}\,\mathrm{d}\sigma\right\}. \quad (4)$$

It is necessary to compensate delay of one the two beams with respect to the other one when recording the interferogram because the coherence length, in wide band, is only a few fringes. Monochromatic waves coherently interfere around the equal optical path position when the optical paths of the two beams are matched by a delay line.

The first term in Eq. (4) will be left aside in the following and I will only consider the second one which is the modulated part of the interferogram. When the complex spectrum is defined as the hermitian part of the spatio-temporal source spectrum (modulus is an even function and phase is an odd function of wavenumber):

$$B_{\mathrm{c}}(\sigma) = \frac{1}{2}\left(B(-\sigma)V_{12}(-\sigma) + B(\sigma)V_{12}^*(\sigma)\right), \quad (5)$$

the modulated part of energy, noted $\mathcal{I}(x)$, gets a more convenient expression:

$$\mathcal{I}(x) = \int_{-\infty}^{+\infty} B_{\mathrm{c}}(\sigma)\mathrm{e}^{2j\pi\sigma x}\,\mathrm{d}\sigma. \quad (6)$$

In other words, the Fourier transform of the modulated interferometric signal is the complex spectrum of the astronomical source.

2.2. Double Fourier interferometry

A few different ways of doing interferometry (mostly depending on measured quantities) exist (see review by M. Shao 1992). Some interferometers recombine beams in the pupil plane whereas others are image plane oriented. Here, no distinction will be made between these two different philosophies. Some interferometers (type I) are operated in the long exposure mode, that is to say that a servoed delay line sets the optical path difference (thereafter opd) to a constant value allowing the integration of the interferometric signal to achieve high signal to noise (S/N) ratios on fringe modulation. The value of the opd can be varied to scan through the whole interferogram. Type II interferometers can be considered as short exposure interferometers. The interferogram is acquired during a continuous scan of the opd which is produced either by the Earth's rotation or by a translating retroreflecting unit moving at a constant speed or by a combination of the two. Integration is then no longer possible. Type I interferometers are not opd fluctuation sensitive as the opd is servoed, whereas many factors can introduce opd fluctuations in type II interferometers (this point will be adressed in Sect. 2.3). Type II interferometers are dedicated to spectral data analysis for they naturally reach a higher spectral resolution while type I data are reduced in direct space. These type II interferometers are called Double Fourier Interferometers (hereafter DFI) because they both probe spatial and temporal coherence properties of the light emitted by astrophysical sources (Itoh & Ohtsuka 1986; Mariotti & Ridgway 1988). Spatial information is contained in the modulated energy of interferograms as shown in Sect. 2.1 and is wavelength dependent. The Fourier transform of the interferogram sequence yields the source temporal spectrum rescaled by the visibility function. It has been shown (Ridgway et al. 1986) that an accurate knowledge of the visibility-wavelength relation would have fruitful astrophysical implications, as well as visibility as a function of spatial frequency. DFI

[2] More precisely, visibility moduli are straightforewardly measured by interferometers, a more indirect procedure is used for measurements of visibility phases, what is measured is the sum of three phases for a three-telescope loop which is called phase closure, this special technique was designed to cancel out additionnal phase errors, see references thereafter in the paper.

allows the determination of the visibility as a function of wavelength and is the interferometric mode that is mostly concerned in the following of the paper.

2.3. Optical path fluctuations and phase information loss

As shown in Eq. (6) an interferogram can be considered as a temporal sequence whose Fourier transform is proportionnal to the spectrum of the source. The two conjugate variables are the opd (or time) in the direct space and wavenumber (or frequency) in the Fourier space; one shifts from one set of conjugate variables to the other by multiplying or dividing by the speed of the fringes. Thus opd varies linearly with time. This is what one should expect in an ideal interferometer. In reality this occurs in a different way. Opd does not vary linearily with time. Some opd distortions are introduced and have mechanical and atmospheric sources. Vibrations of static optics on the beam path change its length and make it oscillate. But they can be lowered to an inoffensive magnitude by increasing the stiffness of the optics and by absorbing vibrations. Non-linearities in the motion of the retroreflecting stage of the delay line cause opd to fluctuate but they can also be cancelled out by servoing the speed of the carriage supporting the retroreflector. Some fiercer fluctuations are generated by atmospheric turbulence. Here we assume that atmospheric perturbations of wavefronts are reduced to the 0-order ones (the spatially averaged pertubations on the pupil) and that higher orders have been filtered out by using monomode fibers for example (Coudé du Foresto & Ridgway 1991; Coudé du Foresto et al. 1992), by data reduction or with adaptive optics. The 0-order term is known as "piston effect" and opd fluctuations are due to differential piston between two apertures of the interferometer. But piston and differential piston stand for the same physical phenomenon.

Opd fluctuations result in the loss of the Fourier relation between the spectrum and the interferogram sequence preventing physical information recovery from the spectrum. Figure 3 of Sect. 3 shows four simulated low resolution spectra. The first one is computed from an opd fluctuation free interferogram whereas the others simulate observed spectra with regular turbulence conditions. It is obvious that without any piston correction no accurate information can be extracted from these spectra. Besides, piston introduces a random shift of the central fringe of the interferogram preventing measurement of the exact phase of visibilities, the accurate knowledge of which being essential to reconstruct a high resolution image of the source.

If most sources of optical path fluctuations have negligeable effects, atmospheric turbulence effects at optical wavelengths must be taken into account. It is possible to artificially increase the length of coherent interferogram by scanning at a high speed. Rapid scanning freezes piston but it does not reduce its amplitude. Besides, fast scanning reduces the instrumental visibility (hence the S/N ratio of the modulated signal) as the detector response decreases with increasing frequencies. Turbulence opd fluctuations thus turn out to be a strong limitation to optimum information extraction in optical astronomical interferometry. In the following Sects. I will expose a method to correct "pistoned" interferograms to retrieve the modulus of the spectrum and the phase to within a constant. This method does not take into account the possibility to retrieve the exact phase of visibilities and does not address the issue of image reconstruction in interferometry.

3. Statistical and temporal properties of atmospheric optical path fluctuations

This section is dedicated to the characterisitics of piston. The features are used in paragraph 3.6 to simulate piston and pistoned interferograms.

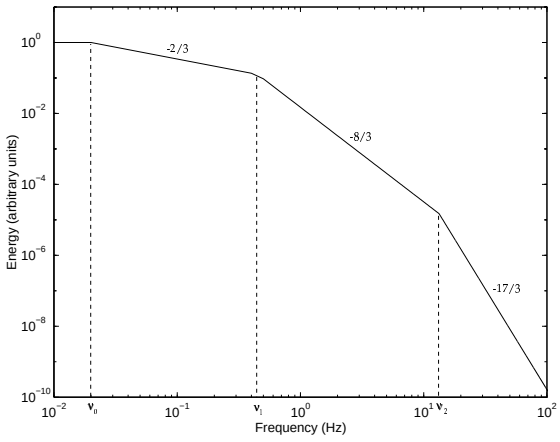

Fig. 1. Differential piston power spectrum

3.1. Statistical properties of differential piston

A complete study of statistical properties of turbulence effects can be found in Roddier (1981) from which this paragraph is inspired.

Astronomical beams travelling through the turbulent atmosphere on their way to the aperture traverse a succession of thin independent turbulent layers each with a fluctuation statistics. Resulting from the central limit theorem, the overall statistics are Gaussian and are fully determined by the standard deviation. This thus applies to optical path fluctuations statistics. The standard deviation value a priori depends on wavelength λ, fried parameter r_0 and baselength D. Its expression in meters is:

$$\sigma_\epsilon = \frac{2.62}{2\pi}\ \lambda\left(\frac{D}{r_0}\right)^{5/6} \tag{7}$$

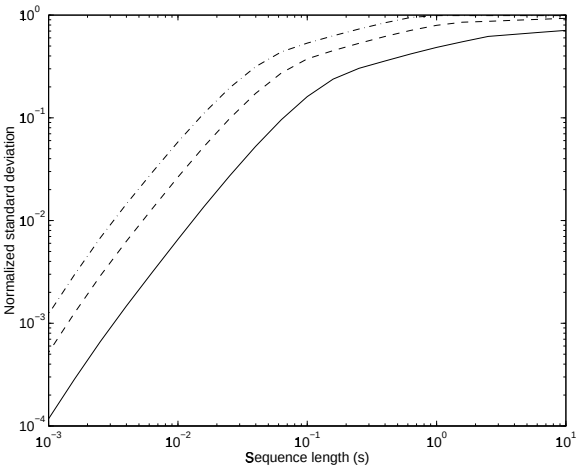

Fig. 2. Effective standard deviation of piston for temporal sequencies of finite length. The standard deviation is normalized to unity for a sequence of infinite duration. Curves are plotted for three different wind speeds: 10 m s^{-1} (full line), 20 m s^{-1} (dashed line) and 30 m s^{-1} (dashed and dotted line)

where the subscript ϵ refers to the opd fluctuation standard deviation. It is interesting to realize the importance of this effect. Assuming correct seeing conditions for observing with $r_0 = 60$ cm at 2.2 μm and that the interferometer baseline is $D = 21.2$ m, the standard deviation for opd fluctuations is 18.5 μm that is about 9 fringes in the K photometric band (to be compared to the coherence length of 10 fringes) and an error of 56 radians on visibility phase measurements. Since r_0 is proportionnal to $\lambda^{6/5}$, σ_ϵ does not depend on wavelength and piston is an achromatic effect. The reduction method proposed in this paper mainly relies on this critical property of atmospheric differential piston.

3.2. Temporal properties of differential piston

Let us now focus on the evolution of differential piston with time. A theoretical average spectrum is given in Conan et al. (1992) for an infinite outer scale. It is a three-slope spectrum in Log-Log representation with cut-off frequencies depending on the average speed of turbulent layers v as defined in Roddier (1981), also depending on the baselength D and the diameter of the pupils d. These frequencies have the following expressions:

$$\begin{aligned} \nu_1 &= 0.5\frac{v}{D}, \\ \nu_2 &= 0.3\frac{v}{d}, \end{aligned} \tag{8}$$

and the slopes are typical of a Kolmogorov turbulence: $-2/3$, $-8/3$ and $-17/3$. Considering parameters given in Colavita et al. (1987) for observations carried out at the Mark III interferometer with a 12 m baselength, a 14 m s^{-1} average wind speed and 2.5 cm apertures, cut-off frequencies are 0.6 and 168 Hz which is in good agreement with the piston power spectra published in this paper (the data are in the range 0.001 − 100 Hz and do not display the third slope feature).

3.3. The outer scale of turbulence

The idealized temporal and statistical properties given before are correct to a certain extent. They require the outer scale of turbulence (scale at which turbulent energy is introduced in the atmosphere) to be infinite. The relation in Eq. (7) saturates for baselines larger than the outer scale and energy in the power spectrum saturates at low frequencies. Recent measurements of the outer scale at the SUSI interferometer site in Australia (Davis et al. 1995) for baselines ranging between 5 and 80 m state values of about a few meters. Piston measurements show that relation (7) departs from linearity in Log-Log coordinates (Fig. 3 of that paper) – for the 20 m baseline, the measured piston standard deviation is 8.4 μm whereas the expected value is in the range 16 − 30 μm, depending on seeing conditions – and power spectra level out for frequencies below $\simeq 0.02$ Hz. Although there is a controversy about the outer scale (references can be found in Davis et al.) it turns out that a finite range is more likely than an infinite one and that methods based on predictions from the power spectrum at low frequency that found an infinite outer scale are not reliable because they are consistant with a wide range of results. Direct measurements with different baselines are definitely likely to be a good basis for a good understanding of the properties of piston. As a consequence, the power spectrum used in this paper, taking into account a finite outer scale, is a four slope spectrum in a Log-Log diagram with a low cut-off freqeuncy at 0.02 Hz and the two cut-off frequencies predicted by Conan et al. (1992). It is plotted in Fig. 1.

3.4. Differential piston for finite length sequences

Prediction of piston standard deviation by Roddier (1981) applies to sequences of infinite duration. In real life, interferometric scans are finite in length and, since piston speed is not infinite, standard deviation on a finite length is necessarily lower than the prediction. For a sequence of duration T frequencies below $\frac{1}{T}$ are atttenuated thus decreasing standard deviation. In Appendix A the analytical expression of standard deviation is given as a function of scan duration. The result is plotted in Fig. 2 for observing parameters given in Table 1 for three wind speeds (10, 20 and 30 m s^{-1}) spread across the range of observed speeds in good astronomical sites (E. Gendron, private communication). Standard deviation for infinite sequence lengths is normalized to unity. With $v = 20$ m s^{-1} and for durations in the range 0.1 − 1 s standard deviation is proportionnal

to $T^{\frac{1}{3}}$ whereas it is proportionnal to $T^{\frac{5}{3}}$ for shorter durations. In short, attenuation of piston variations becomes important for sequences shorter than $\frac{1}{\nu_2}$. It is interesting to derive the coherence time of piston to get a rough estimate of the time scale necessary for a piston peak-to-peak variation. In the same conditions as those used above, the coherence time is found to be:

$$\tau_\epsilon = 31.5\,\mathrm{ms}, \tag{9}$$

which means that piston varies slowly and that it has to be determined on long sequences to be averaged out.

3.5. Discussion

Both piston amplitude and temporal behavior are well known thus allowing realistic simulations as will be shown in the next section. Interferometer sensitivity to piston is wavelength dependent. The shorter the wavelength, the higher the fringe frequency for a given fringe speed, hence the higher the effective piston coherence time. But, as far as piston amplitude is concerned, the shorter the wavelength the higher the relative amplitude of optical path fluctuations. It is of a great interest to know whether a numerical piston correction method is more efficient improving amplitude or time coherence. Let us consider sinusoidal optical path fluctuations as in Brault (1985) of frequency ω and amplitude δ. In the spectral domain, these fluctuations produce two symmetric replicas of the spectrum shifted by ω and $-\omega$ and of relative height δ. This simple example shows that it is more profitable to reduce piston amplitude to achieve spectrum restoration as the noise introduced by piston is proportionnal to its amplitude. It also demonstrates that infrared wavelengths are more suitable for DFI than visible wavelengths.

3.6. Simulations of pistoned interferograms

The simulations presented in this paper are in the K photometric band centered at $2.2\,\mu$m. The simulated interferometer is the fibered recombination unit FLUOR at the focus of the IOTA interferometer as explained in Perrin et al. (1995). The characteristics of the inteferometer are listed in Table 1. The source is supposed to be unresolved at any wavelength in the band yielding a constant visibility of 1. The spectrum is a spectrum of a blackbody at 3500 K seen through aK filter.

There are 1024 samples per sequence. Given the average wind speed v, the scanning frequency ν_f, I first compute a Gaussian sequence of average 0 and of standard deviation 1. This sequence is filtered with the piston power spectrum given in Sect. 3.2 and is normalized to a standard deviation of σ_ϵ attenuated by the factor given by curves in Fig. 3. The length of each sequence is $400\,\mu$m corresponding to a scan duration of 160 ms and yielding an attenuation factor of 0.57 and a standard deviation of $10.5\,\mu$m. This final sequence is the opd fluctuation as a function of opd x: $\epsilon(x)$. I then compute the nominal interferogram $I(x)$ given in Eq. (4) and normalized to an average of 1. Eventually, the pistoned interferogram is $I_\mathrm{p}(x) = I(x + \epsilon(x))$. In interferometers, the zero opd is computed relative to the knowledge of the metrology of the system. It is known to within a constant which is the instrument opd. We assume in the following that the instrument opd is zero (we only consider the errors due to the atmosphere).

Table 1. Simulation parameters

FLUOR-IOTA hardware caracterisitics	
baselength (D)	21.2 m
wavelength (λ_0)	$2.2\,\mu$m
apertures diameter (d)	0.45 m
Nominal parameters	
Fried parameter (r_0)	60 cm
wind speed (v)	$20\,\mathrm{m\,s^{-1}}$
fringe speed (v_f)	$5\,\mathrm{mm\,s^{-1}}$
fringe frequency (ν_f)	2274 Hz
saturation frequency (ν_0)	0.02 Hz
low cut-off Kolmogorov frequency (ν_1)	0.45 Hz
high cut-off Kolmogorov frequency (ν_2)	13.33 Hz

Figure 3 displays a set of four interferograms simulating an observation of a 3500 K blackbody spectrum star with a resolution of $25\,\mathrm{cm^{-1}}$. On each line the first graph is the interferogram followed by the modulus of the spectrum, the phase of the spectrum and the piston sequence. The speed of the fringes is $5\,\mathrm{mm\,s^{-1}}$ yielding a fringe frequency of 2274 Hz. The wind speed is $20\,\mathrm{m\,s^{-1}}$. The observing conditions are supposed to be quite good with $r_0 = 60$ cm at $2.2\,\mu$m, hence a seeing of 0.7 arcsec. These parameters are hereafter referred to as the nominal parameters and are listed in Table 1.

The first interferogram is not pistoned. When comparing the pistoned ones to this one it is obvious that the speed of the fringes is varying, some fringes being stretched while others are compressed (hence the analogy with the mechanics term "piston"), and that the whole interferogram is shifted with a random position offset. The shape of the modulus of the spectrum has changed. When piston is accelerating in the main lobe of the interferogram, fringes are compressed which increases their apparent frequency. The spectrum support is then shifted to higher frequencies and enlarged as the envelope of the fringes is tightened. This is what can be seen on the second sequence. The opposite behavior is seen on the third sequence where piston is decelerating. The first derivative of piston thus shifts the interferogram in the frequency domain. Higher orders even destroy low resolution information as shown by the simulations. In the fourth sequence, the main lobe of fringes is only slightly pistoned as it has been recorded

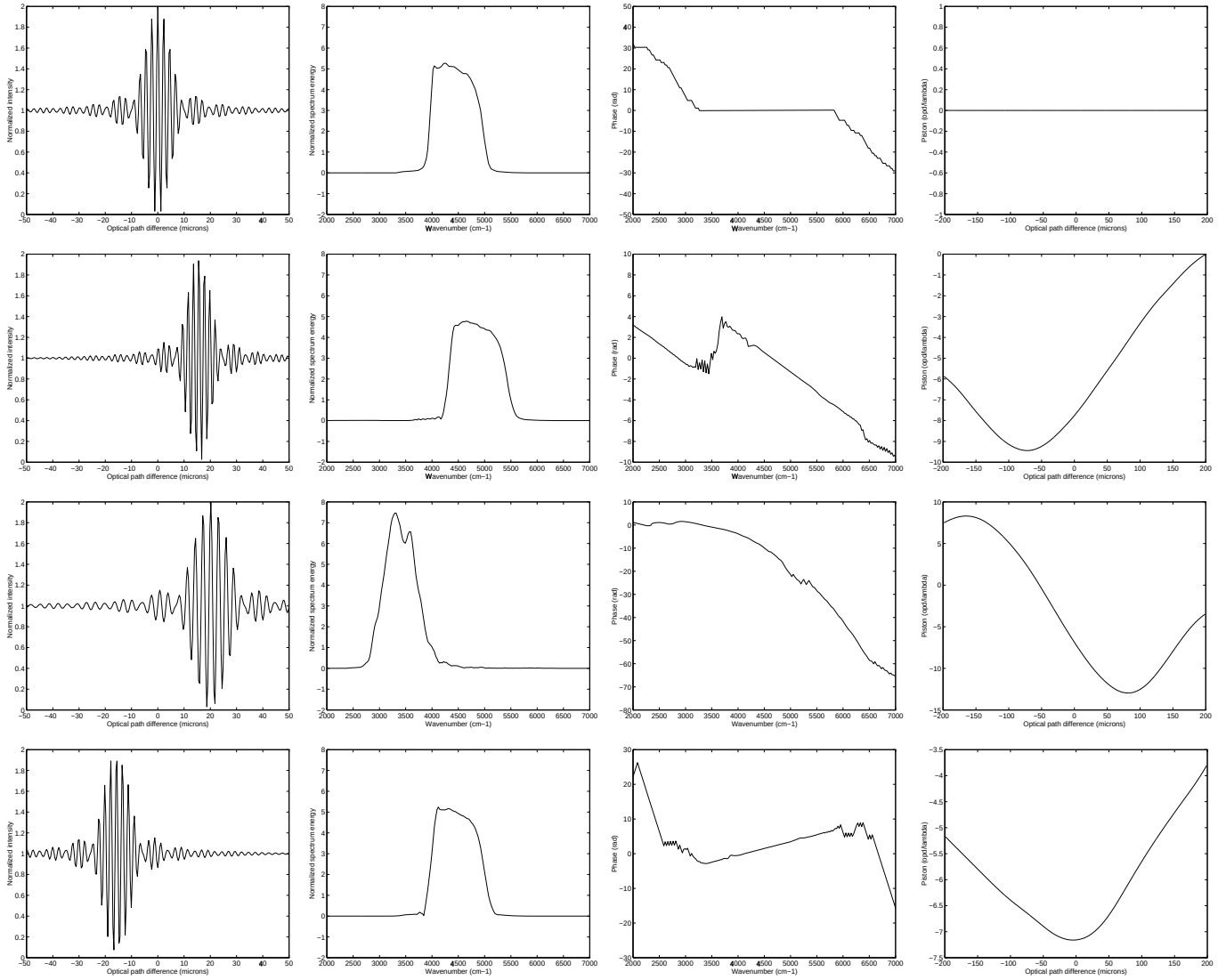

Fig. 3. Simulations of interferometric observations with atmospheric optical path fluctuations. Each line corresponds to a different piston sequence. For each sequence the interferogram, the modulus of the spectrum, the phase of the spectrum and the piston perturbation are plotted

during a phase when piston was flat. Its support is in the correct range but the spectral information is destroyed. Concerning phase, it is constant in the original interferogram whereas it is a function of wavelength in the pistoned ones. It is dominated by a linear component because of the position offset, but some higher order terms are introduced and are due to the asymmetry of the interferograms.
These simulations clearly show that there is a poor correlation between successive pistoned spectra and that spectral information such as line strength cannot be recovered in a direct manner. Let us now focus on a method to retrieve spectral information.

4. Statistical reduction of differential piston

The reduction method which is developped in the following is based on an analytic expression of the fringe packet by means of a Fourier analysis. It does not rely on any model and is thus valid for any geometry of the source. The first part of this section is dedicated to the definition, the calculus and the computation of the phase function. In the second part the problem of reduction is addressed.

4.1. The phase function

4.1.1. Definition

The modulated part of the interferogram as defined by Eq. (6) can be written as the product of a slowly varying

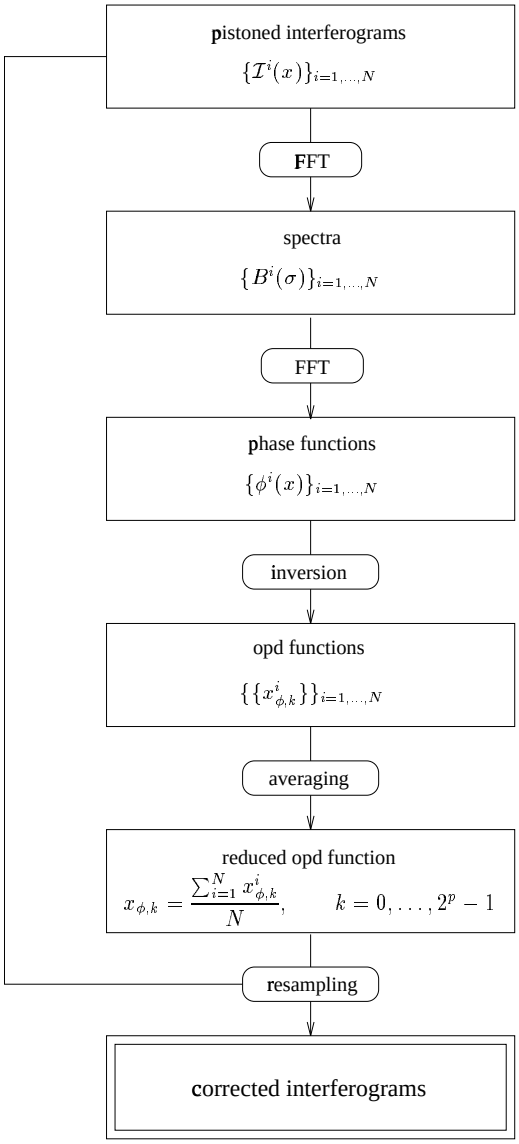

Fig. 4. Algorithm for the correction of the piston effect

positive function, the envelope, by a rapidly oscillating function:

$$\mathcal{I}(x) = \rho(x)\ \cos(\phi(x)), \tag{10}$$

where $\phi(x)$ is the phase function. ϕ can be defined in different ways as it is the argument of a cosine function. For the purpose of the correction algorithm it will be a monotonic, strictly increasing function. It is not continuous and makes jumps of π when the envelope becomes zero and has no derivative.

4.1.2. Calculus

The interferogram of Sect. 2 was defined in wide band but is band limited as the light is filtered. For σ_0, a wavenumber within the support of the one-sided spectrum or the

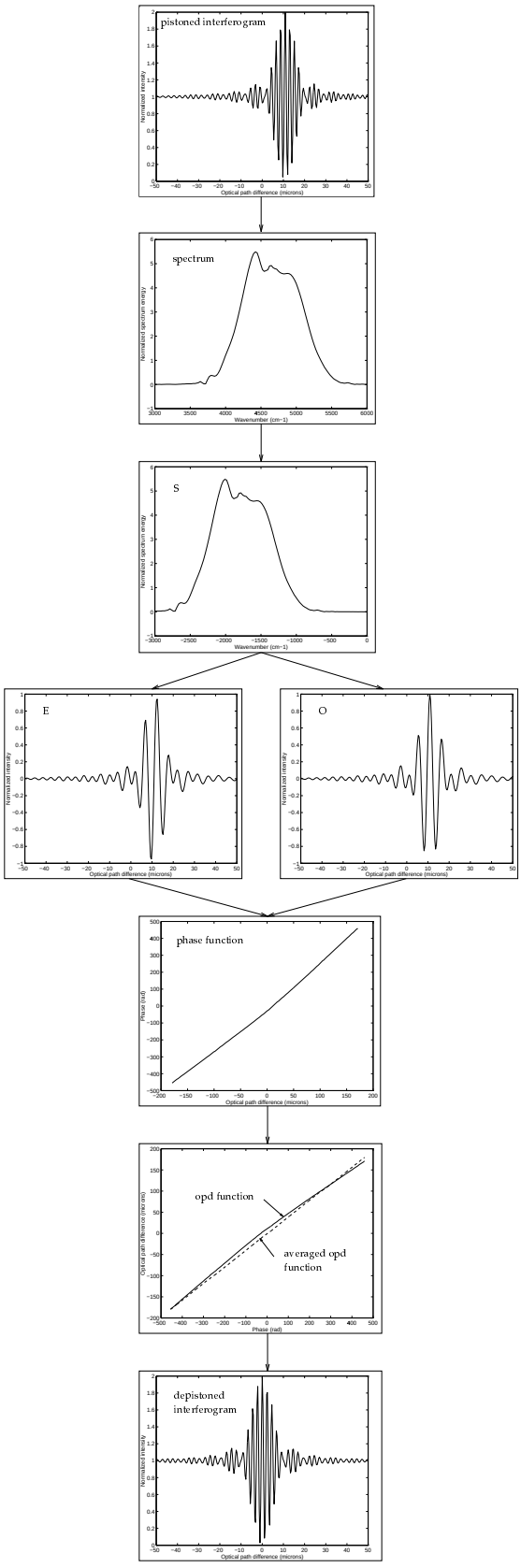

Fig. 5. Sequence of functions computed to resample the interferograms with an opd corrected of the piston effect as defined by the algotihm of Fig. 4

spectrum defined for positive wavenumbers, I define the shifted spectrum S by:

$$S(\sigma) = B(\sigma+\sigma_0)\ V_{12}^*(\sigma+\sigma_0). \tag{11}$$

The complex spectrum is now expressed with the shifted spectrum:

$$B_c(\sigma) = \frac{1}{2}\left(S(\sigma-\sigma_0) + S^*(-\sigma-\sigma_0)\right). \tag{12}$$

This yields a new expression for Eq. (6):

$$\begin{aligned}\mathcal{I}(x) \ &= \ \frac{1}{2}\mathcal{F}^{-1}\left[\mathcal{S}(\sigma)\right](x)\mathrm{e}^{2i\pi\sigma_0 x} + \\ &\quad \frac{1}{2}\mathcal{F}^{-1}\left[\mathcal{S}^*(-\sigma)\right](x)\mathrm{e}^{-2i\pi\sigma_0 x},\end{aligned} \tag{13}$$

where $\mathcal{F}$ is the Fourier transform operator. Let us now consider the inverse Fourier transforms of the hermitian and anti-hermitian parts of the shifted spectrum, noted respectively E and O, and defined as:

$$\begin{aligned}E(x) \ &= \ \frac{1}{2}\mathcal{F}^{-1}\left[\mathcal{S}(\sigma)+\mathcal{S}^*(-\sigma)\right](x), \\ O(x) \ &= \ \frac{-i}{2}\mathcal{F}^{-1}\left[\mathcal{S}(\sigma)-\mathcal{S}^*(-\sigma)\right](x),\end{aligned} \tag{14}$$

leading to a new expression for the interferogram:

$$\mathcal{I}(x) = E(x)\cos(2\pi\sigma_0 x) - O(x)\sin(2\pi\sigma_0 x). \tag{15}$$

$O(x)$ and $E(x)$ are both functions with real values and are odd and even respectively when the shifted spectrum is real. The expressions of the envelope and the phase function are straightforward:

$$\begin{aligned}\rho(x) \ &= \ \sqrt{E^2(x)+O^2(x)}, \\ \phi(x) \ &= \ 2\pi\sigma_0 x + \arctan\left(\frac{O(x)}{E(x)}\right).\end{aligned} \tag{16}$$

The phase function can be mathematically defined as long as the envelope does not become zero. The problem of properly unwrapping this function will be adressed in the next section. An interesting property can be derived from Eq. (16): the interfringe is constant in the interferogram as long as the O function is a constant and is 0, which is equivalent to saying that the shifted spectrum is an even function. The expression of the phase function does not depend on the choice of the wavenumber σ_0. This property will be used in Sect. 4.2 and is demonstrated in the appendix at the end of the paper.

4.1.3. Computation

As defined by Eq. (16), the phase function is not continous as the arctan function is not continuous and returns values in the interval $]-\frac{\pi}{2},\frac{\pi}{2}[$. The phase is first unwrapped to eliminate discontinuities larger than π. The function that is obtained is globally strictly increasing. Some discontinuities still remain that are not due to the arctan function. They occur at each zero of the envelope when its first dervative is not defined. The mathematical function then makes jumps of $-\pi$ or $+\pi$. In reality these jumps are not resolved when working with finitely sampled interferograms. It is not possible to eliminate them: a pistoned phase function can reproduce a positive unresolved leap. But a negative unresolved leap-like variation cannot be due to piston as variations induced by piston are supposed to be smaller than variations of the nominal opd. To insure the final phase function to be monotonic, the negative leaps are rectified. Numerically, when the negative leap has been detected, 2π is added to the phase function after the leap, the leap itself is transformed into a positive leap by a symmetry with respect to the tangent before the leap. The error made on the phase function after the symmetry is negligeable because the phase function is very close to a straight line when it is continuous (the interfringe is almost constant). After these transformations, the computed phase function is monotonic but is defined with a random additive constant proportional to π. The value of this constant is fixed this way: the value of the phase function must be in $[-\pi,+\pi]$ around the white light fringe.

4.2. Correction algorithm

4.2.1. Philosophy

The piston signal $\epsilon(x)$ is a noise on the variable x, the opd. The idea to correct pistoned inteferograms is to reduce noise on the opd as statistical data reductions are usually processed. The main difficulty is to express the opd as a function of something, that is to say to invert Eq. (16) or part of this equation. To do this it is necessary to find a one-to-one function of opd. This function is the computed phase function which will be thereafter mixed up with the mathematical one, although they are quite different as explained in Sect. 4.1.3. Let us note $\epsilon_p(x)$ the p realization of a piston sequence. The corresponding interferogram, envelope and phase function are indexed with p. From the unicity property of the phase function and the envelope, the expression of the pistoned interferogram is:

$$\mathcal{I}_p(x) = \rho_p(x)\cos(\phi_p(x)), \tag{17}$$

with:

$$\begin{aligned}\rho_p(x) \ &= \ \rho(x+\epsilon_p(x)), \\ \phi_p(x) \ &= \ \phi(x+\epsilon_p(x)).\end{aligned} \tag{18}$$

$\phi = \phi_p(x)$ is invertible as ϕ_p is strictly increasing and so is a one-to-one function. The opd as a function of the phase function can be defined and is noted $x_p(\phi)$. The reduced opd function $\bar{x}(\phi)$ is the average of the realizations of the pistoned opd functions. For an infinite number of realizations the reduced opd function converges to the nominal

opd function. For N realizations of the piston the residual piston in the reduced interferogram is thus reduced by a factor $\sqrt{N}$, the reduced inteferogram being eventually:

$$\mathcal{I}_{\rm r}(\bar{x}) = \rho_(\bar{x})\ \cos(\phi(\bar{x})). \tag{19}$$

4.2.2. Algorithm

For sake of clarity the correction algorithm is summarized in Fig. 4 and the functions used in the reduction process are plotted in Fig. 5. Let us assume that N interferograms have been recorded: $\{\mathcal{I}^i\}_{i\,=\,1,\,\ldots,\,N}$, each of length 2^p corresponding to a fixed nominal opd window width Δx or spectral resolution $\delta\sigma$ with $\Delta x\ .\ \delta\sigma\ =\ 1$. The sampling frequency is at least twice the higher spectral frequency to obey the sampling theorem.

Computation of the phase functions Let us consider the two-sided spectrum obtained by discrete Fourier transforming the interferogram. The frequency samples are $(-2^{p-1}+1)\delta\sigma,\ldots,0,\ldots,(2^{p-1})\delta\sigma$ where $2^{p-1}\delta\sigma$ is the Nyquist frequency. $B(\sigma)\ V_{12}^*(\sigma)$ is extracted from positive frequencies, $B(-\sigma)\ V_{12}(-\sigma)$ from negative frequencies and conjugated. The sum and the difference of the two are computed. $2^{p-2}-1$ and 2^{p-2} long zero sequences are added before and after the two lists to produce the $S(\sigma)+S^*(-\sigma)$ and $S(\sigma)-S^*(-\sigma)$ functions of Sect. 4.1.2 with $\sigma_0 = 2^{p-2}\delta\sigma$ (half the Nyquist frequency). After inverse Fourier transform of these two, the phase function is computed as explained in Sect. 4.1.3.

Inversion of the phase functions The previous step yields N pistoned phase functions. They are all defined in the same temporal window (corresponding to an opd window width Δx) but they do not vary in the same range as the piston randomly shifts the interferograms position in the window. For each realization i of the phase function, the maximum $\phi^i_{\rm max}$ and minimum $\phi^i_{\rm min}$ of the function are computed. The common range of variation of all the phase functions is determined to be: $[\phi_{\rm min},\phi_{\rm max}]$, where $\phi_{\rm min} = \max_{i\,=\,1,\,\ldots,\,N}\phi^i_{\rm min}$ and $\phi_{\rm max} = \min_{i\,=\,1,\,\ldots,\,N}\phi^i_{\rm max}$. This is the maximum common range on which opd functions $x^i(\phi)$ can be defined. The phase functions are linearly interpolated on $\{\phi_k = \phi_{\rm min} + \left(\frac{\phi_{\rm max}-\phi_{\rm min}}{2^p-1}\right)k\}_{k\,=\,0,\,\ldots,\,2^p-1}$ producing a sampled opd function $\{x^i_{\phi,k} = x^i(\phi_k)\}_{k\,=\,0,\,\ldots,\,2^p-1}$ for each interferogram i (the index ϕ means that the opd function definition is relative to the phase function whereas the sampled inteferograms $\{\mathcal{I}^i_k\}_{k\,=\,0,\,\ldots,\,2^p-1}$ are defined for the set of nominal opds $\{x_k = \frac{\Delta x}{2^p}(k-2^{p-1}+1)\}_{k\,=\,0,\,\ldots,\,2^p-1}$). The error introduced by the linear interpolation process is very negligeable because the pistoned phase functions have variations between two sampling opds that are linear with a very good approximation as long as the sampling frequency is chosen far greater than the first cut-off frequency of piston.

Computation of the reduced opd function The opd functions are then reduced by processing:

$$x_{\bar{\phi},k} = \frac{\sum_{i\,=\,1}^{N} x^i_{\phi,k}}{N}, \qquad k = 0,\ldots,2^p-1, \tag{20}$$

yielding an estimation of the opd fluctuations for each interferogram:

$$\delta^i_k = x_{\bar{\phi},k} - x^i_{\phi,k}, \qquad k = 0,\ \ldots,\ 2^p-1. \tag{21}$$

The reduced set of opds width $\bar{\Delta}x = x_{\phi,\bar{2^p}-1} - x_{\bar{\phi},0}$ is smaller than the nominal width Δx which means the spectral resolution has been decreased by the reduction process.

Computation of the "unpistoned" interferograms The result of the three previous steps is the estimation of the opd as a function of the nominal opd: $x_{\bar{\phi}} = x_{\bar{\phi}}(x)$. The reduced interferograms or unpistoned interferograms are the following sets of samples:

$$\{(x_{\bar{\phi}}(x_k),\mathcal{I}^i_k)\}_{k\,=\,0,\,\ldots,\,2^p-1}, \tag{22}$$

where the $x_{\bar{\phi}}(x_k)$ are interpolated from the samples $x_{\bar{\phi},k}$. These sequences are then interpolated to yield regularly sampled interferograms.

4.3. An example of correction

The correction algorithm that has just been presented is used to reduce simulated pistoned interferograms. The source has a 3500 K blackbody spectrum and it is seen through a K filter. It is unresolved with a constant visibility modulus of one and with a constant visibility equal to zero. Most of the energy is in the range $\sigma = 4000$ to $5000\,{\rm cm}^{-1}$. The number of samples is 1024 and the parameters are those listed in Table 1. The length of the sequences and the spectral resolution are the same as in Sect. 3.6. 100 interferograms have been simulated. Figure 6 shows the result of the reduction. The left view of Fig. 6 is the corrected interferogram. The spectrum of the corrected interferogram (full line), the original spectrum (square dots), and the spectrum of the pistoned interferogram (dashed line) are on the right view. In Fig. 7 are plotted one of the simulated piston sequences (dashed line) and the approximation of the error signal (full line) as a result of the reduction process. See Sect. 5 for comments.

4.4. Influence of noises on the correction of the interferorams

4.4.1. Multiplicative noise

The expression of the interferogram given in Eq. (2) requires to assume that the intensity in the two arms does not fluctuate. This situation prevails when using single

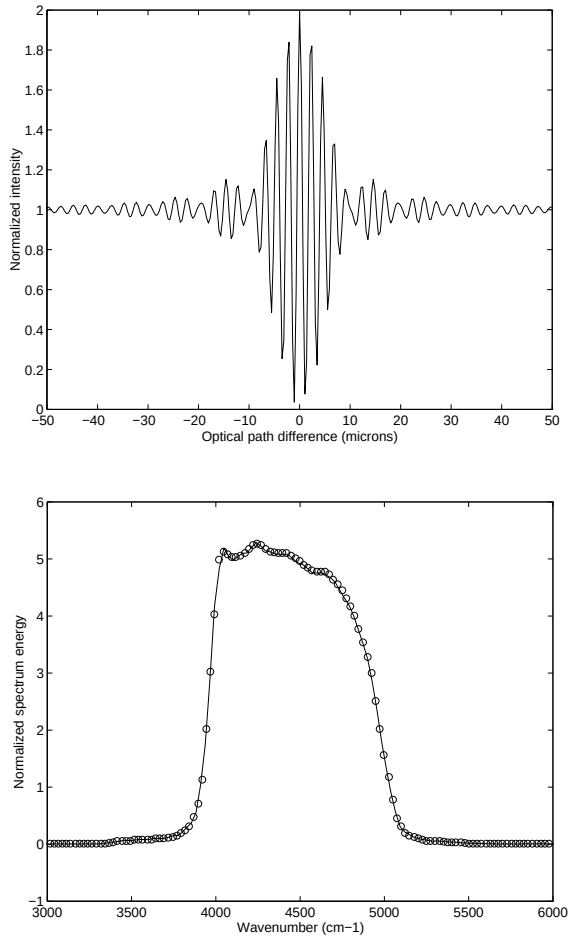

Fig. 6. Corrected interferogram and spectrum for an infinite S/N. Top view: corrected interferogram. Bottom view: spectrum of the corrected interferogram (full line), original spectrum (open circles)

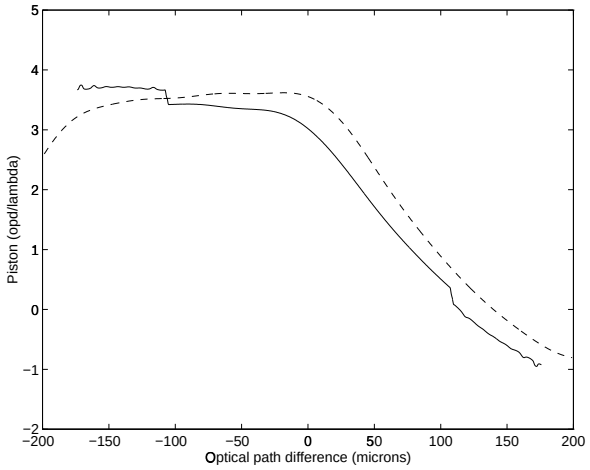

Fig. 7. A simulated piston sequence (dashed line) and the error signal output by the reduction program (full line)

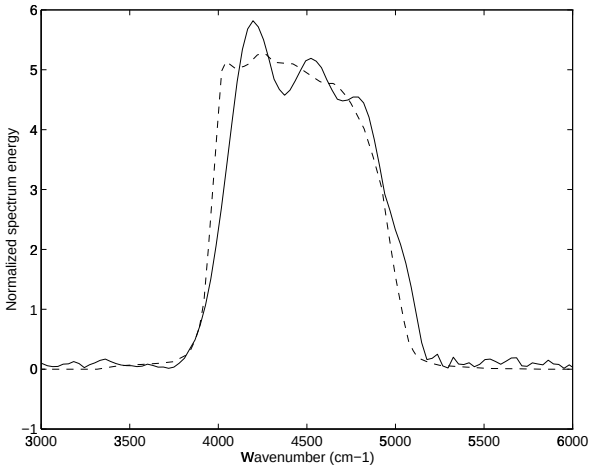

Fig. 8. Spectrum after reduction and summation of 100 interferograms with $S/N = 100$ (the dashed curve is the original spectrum)

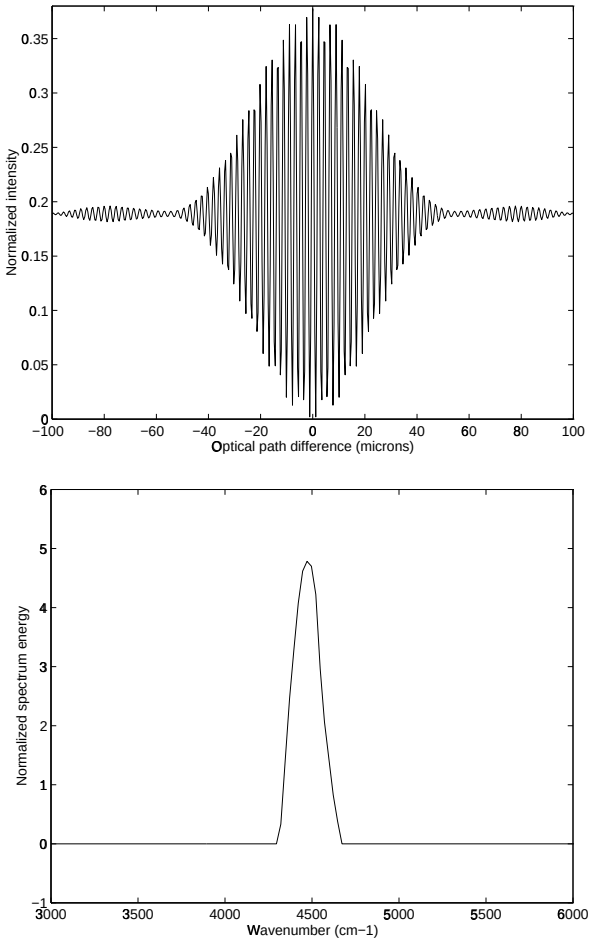

Fig. 9. Simulated interferogram in a narrow K band and spectrum

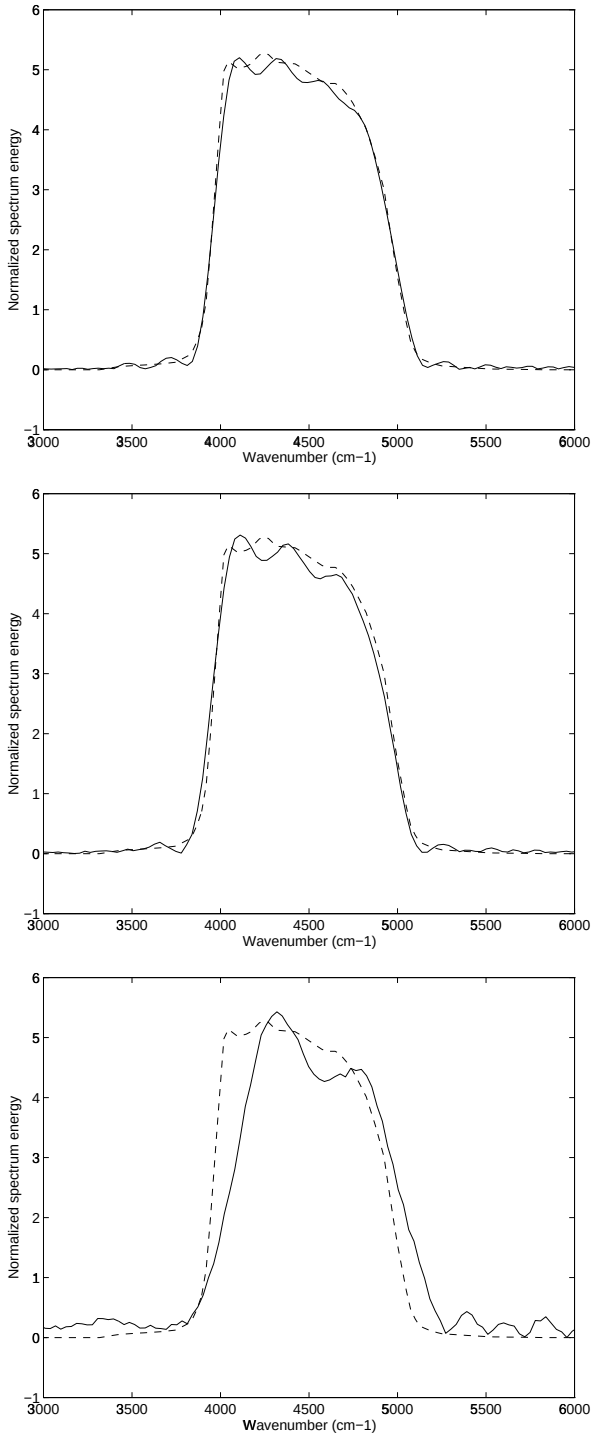

Fig. 10. Spectra of interferograms reduced with the narrow band method for three different S/N ratios. Top view: $S/N = 100$. Middle view: $S/N = 50$. Bottom view: $S/N = 20$. (The dashed curve is the original spectrum)

mode fibers (Coudé du Foresto & Ridgway 1991; Coudé du Foresto et al. 1992) because all coherent photons injected in fibers do interfer and because fibers allow to momitor the fluctuations of photometry in the two arms. The photometric fluctuations are corrected during data reduction and interferograms are renormalized. These variations are low frequency variations (usually of the order of 100 Hz) and the interferograms can be scanned at higher frequencies allowing for a correct filtering to remove these variations if fiber optics are not used. Yet, the visivility transfer function is allowed to vary with time as long as the variations are achromatic. This then only changes the amount of modulated energy but it does not change the phase function. In other words, Eq. (2) can be supposed reliable for the correction algorithm.

4.4.2. Additive noise

The correction simulation of the previous section was carried out assuming an infinite signal-to-noise ratio. The S/N ratio is defined as in Brault (1985): assuming a white noise with rms fluctuations ϵ_x in the temporal domain, the S/N ratio is the ratio of the white fringe amplitude and ϵ_x: $S/N = \frac{\mathcal{I}(0)}{\epsilon_x}$. The local S/N ratio is thus rapidly decreasing in the interferogram with distance to the white light fringe. For the spectrum simulated in this paper, the S/N ratio at the top of the first side lobes is only 15% of the Brault signal-to-noise ratio. Figure 8 shows the modulus of the spectrum after correction of 100 interferograms with $S/N = 100$. After correction of piston, spectra have been averaged to reduce the additive noise. The spectrum correction quality is very degraded because the phase function computed for a local S/N ratio less than 1 is not reliable. Besides, the phase function is very sensitive in the zones where the envelope of the interferogram is zero. As a matter of fact the sign of the interferogram can randomly change there producing random π phase shifts. The more random phase shifts the more different phase functions from one interferogram to the other. Although the main lobe is corrected with a good quality, additive noise is a disaster to correct other lobes when the S/N ratio is not very high, hence the great difference between the corrected spectrum and the original brightness density. Nevertheless, the correction can be improved. The interferometer has two outputs which are theoretically complementary because the input energy is conserved. The detection of the complementary interferogram can be done differently to use it as a correction interferogram. The use of a narrower K filter for the second output will increase the coherence length of the beams, thus widening the envelope of the second interferogram, and will take the first side lobes away, the first lobe width being proportionnal to the inverse of the spectrum width. Assuming the amount of noise is the same in the two arms of the interferometer, the S/N ratio for the narrow filter interferogram is the S/N ratio times the ratio of collected energy through

the K and narrow K filters. The spectrum seen through the narrow K filter with a $25\,\mathrm{cm}^{-1}$ spectral resolution is shown in Fig. 9. The S/N ratio for the narrow band interferogram is approximately degraded by a factor of 5 with respect to the S/N ratio for the regular K filter interferogram. Series of 100 simulated pistoned interferograms have been corrected and averaged for S/N ratios of 100, 50 and 20. The resulting spectra are presented in Fig. 10. It is to be noticed that if filters of adjustable width are available then it is possible to adapt the width of the narrow filter to optimize the final spectral resolution. As a matter of fact, for large S/N ratios in wide band the width of the narrow band can be chosen so that the S/N ratio of the narrow band signal is for example 20 (or larger). The width of the narrow filter is then $\frac{S/N}{20}$ times smaller than that of the wide filter and the resolution of the wide band spectrum is increased by the same factor. If the method is systematically applied then the final resolution is inversely proportional to the S/N ratio of the wide band signal.

4.4.3. Unknown absolute optical path difference

The reduction algorithm has to be adapted when a common origin independent of the interferograms is not known with a precision better than one tenth of a wavelength. A common origin is required for all interferograms to define the position functions. It is very convenient to set the position where the phase function is zero as the origin because it can be very accurately determined. The same algorithm can then be applied, the only difference being that the visibility phase is determined to within a constant and does not allow image reconstruction. Accurate phase recovery will be adressed in another paper.

4.5. Irregularly sampled corrected spectra computation

The correction algorithm of Sect. 4.2.2 has led to the irregularly sampled interferograms of Formula (22). The derivation of spectral information from these sequences is not straightforward. The usual way is to interpolate the irregularly sampled sequences at regularly spaced opds to get regular samples and compute their discrete Fourier transform. The interpolating process introduces an extra noise all the more important as the sampling frequency is lower. This numerical noise can be reduced by oversampling the original sequences to get better estimates when interpolating. The corrected low resolution spectra presented in this paper were obtained using this method. The method fails when high resolution information is mandatory. Oversampling would increase the number of samples without increasing resolution, and very long sequences cannot be oversampled indefinitely. Besides, the residual noise would destroy part of the high resolution information. A method overcoming interpolation drawbacks is necessary. An algorithm has been developped by Feichtinger et al. (1994) to compute spectra from non-uniform samples. The algorithm is iterative and thus slower than the Fast Fourier Transform algorithm. 25 iterations, which is roughly 10^7 floating point operations, are needed to reconstruct the spectrum from 2300 samples with a high accuracy (the normalized error is less than 10^{-13}). The time required by the restoration algorithm increases with the size of the gaps in the samples. The number of iterations would thus increase with the strength of piston.

5. Results

5.1. Reduction of interferograms with an infinite S/N ratio

From the corrected spectrum and interferogram calculated in Sect. 4.3 and presented in Fig. 6, the modulus and the phase of the complex visibility are computed in the range $4000-5000\,\mathrm{cm}^{-1}$ (Fig. 11). The average measured visibility is 1.006 with a standard deviation of 1.3% (Table 2). The phase is almost perfectly zero, the error being less than 0.01 rad. The oscillations in the visibility modulus account for most of the noise. The closer the edges of the spectrum, the bigger the oscillations. The phase is left unaffected by these oscillations. This is the Gibbs phenomenon (Bracewell 1986). As shown in Fig. 7 the injected error signal is well reconstructed by the reduction process on more than $100\,\mu$m on each side around the zero opd position. The difference between the injected error signal and the correction process output error signal is, as expected, of the order of $\frac{\lambda}{2}$ rms. It is a smooth and coherent noise which explains the good reconstruction of the spectrum. A fast varying noise with the same rms fluctuations would produce a spectrum with few similarities with the original one. Before $-108\,\mu$m and after $107\,\mu$m the reconstructed piston signal is shifted by $1\,\lambda$ (or the phase function is shifted by π) with respect to the signal reconstructed in the interval $[-100,+100]$. The interpolations necessary to compute the interferograms with fluctuating opds generate errors in the interferograms that are similar to a noise. The π-leap in the output piston is due to this noise. As a consequence, although the reduced interferogram is defined on a width $\Delta x \simeq 360\,\mu$m, the actual spectral resolution is determined by a width $\Delta x \simeq 200\,\mu$m and is $\delta\sigma \simeq 50\ \mathrm{cm}^{-1}$. It is possible to increase spectral resolution with an infinite S/N ratio if the method explained at the end of Sect. 4.4.2 is extrapolated. The width of the narrow band interferogram is the reverse of the bandwidth and the resolution of the reconstructed wide band spectrum is then of the order of the bandwidth of the narrow band spectrum.

5.2. Reduction of interferograms with finite S/N ratios

More realistic simulations are necessary to determine how good the correction can be when data are noisy and what should be expected with this method. Three S/N ratios

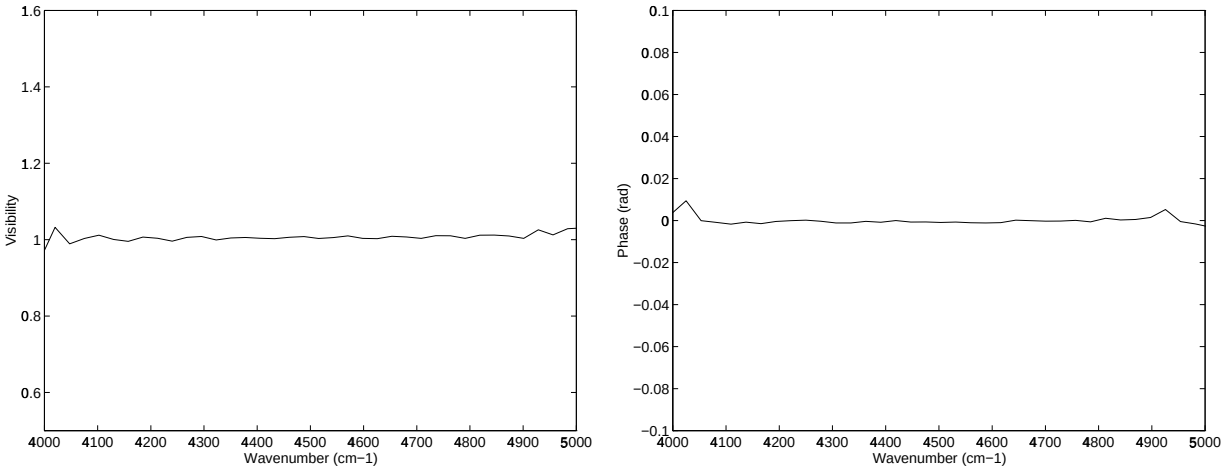

Fig. 11. Visibility modulus (left view) and visibility phase (right view) for an infinite S/N ratio

Table 2. Reduction results

S/N	$+\infty$	100	50	20
V	1.006	1.021	1.044	1.153
σ_V	0.013	0.045	0.047	0.424

have been simulated: 100, 50, 20. The spectrum displayed in Fig. 8, which is the result of the reduction and summation of 100 interferograms with $S/N = 100$, shows the limits of the method in its basic use. For such a S/N ratio the spectrum reconstruction starts to be of poor quality and the inferred visibility function gets less and less reliable. Spectra obtained with the narrower filter method of Sect. 4.4.2 and displayed in Fig. 10 lead to the visibility functions moduli and phases of Fig. 12. As for the case of the infinite S/N ratio, the Gibbs phenomenon is visible. Spectral fluctuations frequencies decrease with decreasing S/N ratios indicating that spectral resolution is also decreasing, and fluctuations amplitudes increase with noise. The statistics of the moduli of the measured visibility functions are presented in Table 2. Visibility functions are measured with a quite good accuracy for S/N ratios of 100 and 50 with average precisions of 2.1% and 4.4% respectively. Because of the Gibbs phenomenon, local errors can be larger than 10% on the edge of the spectrum. For $S/N = 20$ the correction algorithm fails to reconstruct workable visibility moduli. As far as phases are concerned, the reconstruction is easier. The maximum error is 0.01 rad for $S/N = 100$ and 50 and it reaches 0.02 rad for $S/N = 20$.

5.3. Concluding remarks

From these results a few conclusions can be drawn on what can be expected from the piston reduction process. First, in the simulations the fringes were scanned at 5 mm s^{-1} corresponding to a fringe frequency of 2274 Hz at 2.2 μm. For a scan length of 400 μm it has been shown that the standard deviation of piston is 10.5 μm for average atmospherical conditions on the IOTA interferometer and for this fringe speed. Each set of simulated data is a record of 100 interferograms. After reduction the strength of piston is thus attenuated by a factor of 10 and the standard deviation of optical path fluctuations is $\frac{\lambda}{2}$ at 2.2 μm. The good quality of the correction obtained with the proposed algorithm in realistic conditions of observation shows that it is workable for real observations. Second, very good S/N ratios are necessary if visibility measurements with precisions better than 5% are required. It turns out that the maximum level of noise that makes this goal achievable corresponds to a S/N ratio close to 50. Third, this method necessarily degrades the initial spectral resolution. After correction, the estimated resolution for an infinite S/N ratio is about 50 cm^{-1} and is of the order of 100 cm^{-1} or more for S/N ratios of 100 and 50. These resolutions are poor relative to the resolutions needed for a fruitful analysis of CO lines in the K band for example. Nevertheless, although it is theoretically possible to indefinitely increase spectral resolution in the case of an infinite S/N ratio as explained in Sect. 5.1, with these resolutions it is possible to derive gradients and higher order terms from the computed visibilities that should contain interesting informations.

6. Conclusion

Interferometric measurements of fundamental parameters of stars are common applications of astronomical interferometers in the optical range. What is measured is the average value of parameters across a spectral band. Knowledge of the dependence of these parameters with wavelength would be precious and would bring rich informations on

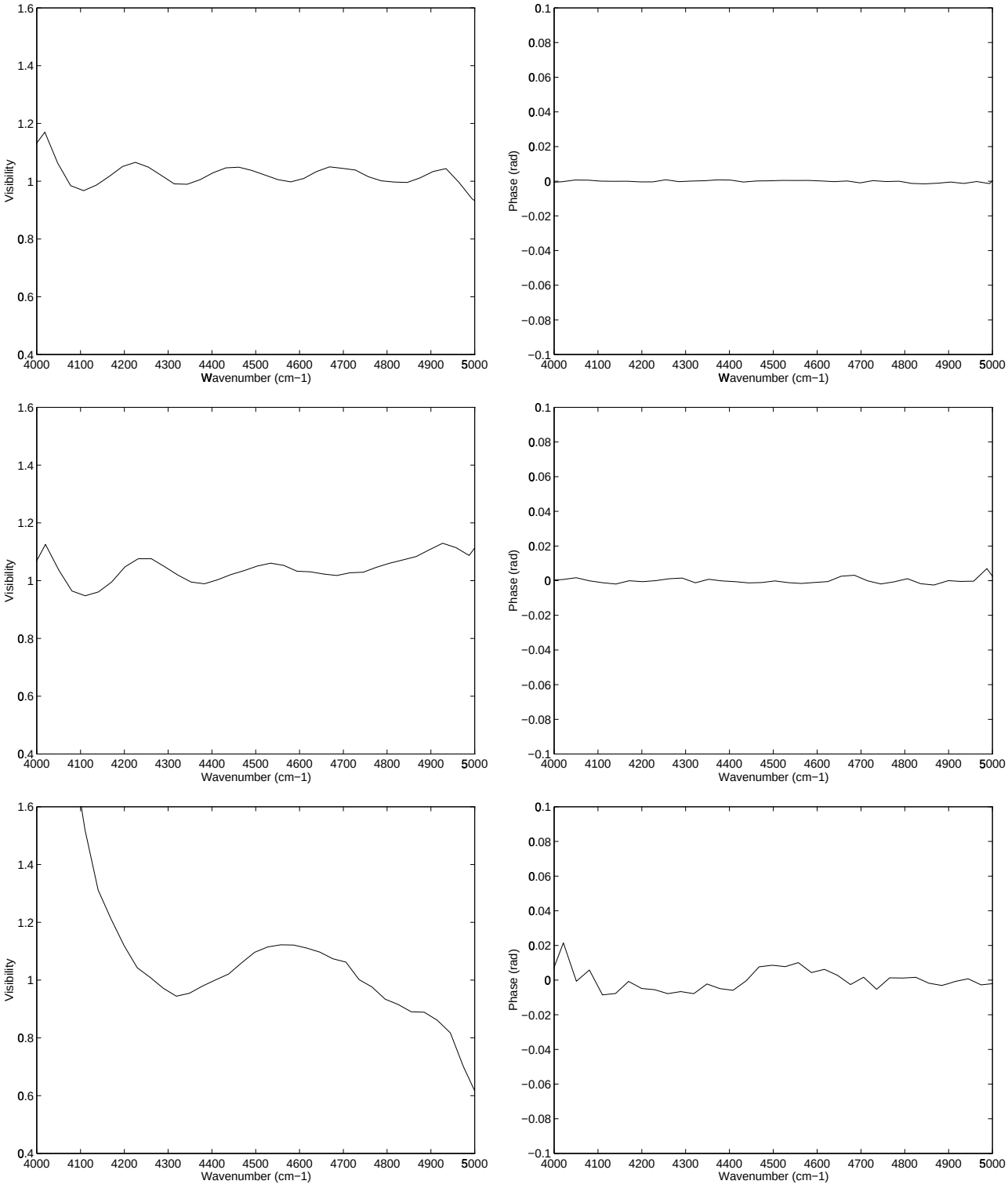

Fig. 12. Visibility moduli (left views) and phases (right views) for S/N of: 100 (top views), 50 (middle views) and 20 (bottom views)

the physical conditions of the sources. A fundamental limitation to achieve this goal is the atmospheric phenomenon of optical path fluctuations or piston effect. It has been shown that the method presented in this paper allows to recover the visibility function with a low spectral resolution. Visibility moduli are reconstructed with a precision that can be as good as a few percent between 2 and 2.5 μm for S/N ratios greater than 50. Visibility phase gradients are also very well extracted from the simulated data with errors that are less than 0.01 rad.

This reduction algorithm for correction of piston fails to recover the true phase of visibilities. This is not prejudicial to the spectral analysis of visibilities. A complement to this algorithm is needed if one wants to remove atmospheric phase errors from interferometric data to achieve high resolution imaging and will be presented in a forthcoming paper.

Appendix A

Supposing a piston sequence of duration T. Let us define the standard deviation of piston during that sequence:

$$\sigma(T) = \sqrt{\frac{1}{T}\int_{-\frac{T}{2}}^{+\frac{T}{2}} \left(\epsilon(t) - \bar{\epsilon}\right)^2 \,\mathrm{d}t}, \tag{23}$$

where $\bar{\epsilon}$ is the average value of piston:

$$\bar{\epsilon} = \frac{1}{T}\int_{-\frac{T}{2}}^{+\frac{T}{2}} \epsilon(t)\,\mathrm{d}t. \tag{24}$$

Let us consider the T-periodic function:

$$\gamma(t) = \left[\epsilon(t)\ .\ \Pi_T(t)\right] \star \sqcup\!\sqcup_T\,(t), \tag{25}$$

where Π_T and $\sqcup\!\sqcup_T$ are, respectively, the window function of width T and the Dirac comb with spacing T. Then, γ equals ϵ on the interval $\left[-\frac{T}{2}, +\frac{T}{2}\right]$ and the moving average:

$$a(t) = \frac{1}{T}\int_{t-\frac{T}{2}}^{t+\frac{T}{2}} \gamma(x)\,\mathrm{d}x \tag{26}$$

is a constant equal to $\bar{\epsilon}$ by definition of γ. Besides, the moving average acts as a low pass filter with transfer function $\frac{\sin(\pi\omega T)}{\pi\omega T}$ on γ. It is thus straightforward to derive the spectrum of the periodic function $\Gamma(t) = \gamma(t) - a(t)$ which matches $\epsilon(t) - \bar{\epsilon}$ on $\left[-\frac{T}{2}, +\frac{T}{2}\right]$:

$$\tilde{\Gamma}(\omega) = \left(1 - \frac{\sin(\pi\omega T)}{\pi\omega T}\right)\ .\ \tilde{\gamma}(\omega), \tag{27}$$

with:

$$\tilde{\gamma}(\omega) = \left[\tilde{\epsilon}(\omega) \star \frac{\sin(\pi\omega T)}{\pi\omega T}\right] . \sqcup\!\sqcup_T(\omega). \tag{28}$$

$\tilde{\Gamma}$ has discrete values with spacing $\frac{1}{T}$ and $\tilde{\Gamma}(0) = 0$. Hence, for $\omega \neq 0$:

$$\tilde{\Gamma}(\omega) = \sum_{n=-\infty}^{n=+\infty} \left[\tilde{\epsilon}(\omega) \star \frac{\sin(\pi\omega T)}{\pi\omega T}\right] \left(\frac{n}{T}\right)\ .\ \delta(\omega - \frac{n}{T}) \tag{29}$$

and the spectrum is zero except for harmonics:

$$hn = \int_{-\infty}^{+\infty} \tilde{\epsilon}(\frac{n}{T} - \omega)\ .\ \frac{\sin(\pi\omega T)}{\pi\omega T}\,\mathrm{d}\omega. \tag{30}$$

Computing the standard deviation for a piston sequence of duration T thus amounts to computing the standard deviation of the periodic function Γ which is the square root of the infinite sum of the squared harmonics. Eventually:

$$\sigma(T) = \sqrt{2\sum_{n\ =\ 1}^{n\ =\ +\infty} hn^2}. \tag{31}$$

Appendix B

For two wavenumbers σ_1 and σ_2 I define the corresponding envelopes ρ_1 and ρ_2, the phase functions ϕ_1 and ϕ_2, the shifted spectra S_1 and S_2, the odd and even functions O_1 and O_2, E_1 and E_2. By definition, there is a simple relation between S_1 and S_2:

$$S_2(\sigma) = S_1(\sigma + \sigma_2 - \sigma_1). \tag{32}$$

Let us derive the expression of E_2:

$$\begin{aligned}
E_2(x) &= \frac{1}{2}\mathcal{F}^{-1}\left[S_2(\sigma) + S_2^*(-\sigma)\right](x) \\
&= \frac{1}{2}\mathcal{F}^{-1}\left[S_1(\sigma + \sigma_2 - \sigma_1) + S_1^*(-\sigma + \sigma_2 - \sigma_1)\right](x) \\
&= \frac{1}{2}\mathcal{F}^{-1}\left[\mathcal{S}_1(\sigma)\right](x)\mathrm{e}^{2i\pi(\sigma_1-\sigma_2)x} + \\
&\quad \frac{1}{2}\mathcal{F}^{-1}\left[\mathcal{S}_1^*(-\sigma)\right](x)\mathrm{e}^{-2i\pi(\sigma_1-\sigma_2)x} \\
&= E_1(x)\cos(2\pi(\sigma_1 - \sigma_2)x) - O_1(x)\sin(2\pi(\sigma_1 - \sigma_2)x).
\end{aligned} \tag{33}$$

In the same way it can be shown that:

$$O_2(x) = O_1(x)\cos(2\pi(\sigma_1-\sigma_2)x) + E_1(x)\sin(2\pi(\sigma_1-\sigma_2)x). \tag{34}$$

As a consequence, it is obvious that the envelopes are the same:

$$\rho_1(x) = \sqrt{E_1^2(x) + O_1^2(x)} = \sqrt{E_2^2(x) + O_2^2(x)} = \rho_2(x). \tag{35}$$

Let us show that the two calculi lead to the same phase function:

$$\begin{aligned}
\phi_2(x) &= 2\pi\sigma_2 x + \arctan\left(\frac{O_2(x)}{E_2(x)}\right) \\
&= 2\pi\sigma_2 x + \\
&\arctan\left(\frac{O_1(x)\cos(2\pi(\sigma_1 - \sigma_2)x) + E_1(x)\sin(2\pi(\sigma_1 - \sigma_2)x)}{E_1(x)\cos(2\pi(\sigma_1 - \sigma_2)x) - O_1(x)\sin(2\pi(\sigma_1 - \sigma_2)x)}\right) \\
&= 2\pi\sigma_2 x + \arctan\left(\frac{\frac{O_1(x)}{E_1(x)} + \tan(2\pi(\sigma_1 - \sigma_2)x)}{1 - \frac{O_1(x)}{E_1(x)}\tan(2\pi(\sigma_1 - \sigma_2)x)}\right) \\
&= 2\pi\sigma_2 x + \arctan\left(\tan\left[\phi_1(x) - 2\pi\sigma_1 x + 2\pi(\sigma_1 - \sigma_2)x\right]\right) \\
&= \phi_1(x).
\end{aligned} \tag{36}$$

The previous lines thus demonstrate that the envelope and the phase function do not depend on the choice of the shifting wavenumber. The derivation is still valid with $\sigma_0 = 0$. In this case $\mathcal{I}(x) = E(x)$ and:

$$\begin{aligned} \rho(x) &= \sqrt{E^2(x) + O^2(x)}, \\ \phi(x) &= \arctan\left(\frac{O(x)}{E(x)}\right). \end{aligned} \tag{37}$$

References

Baldwin J.E., Haniff C.A., Mackay C.D., Warner P.J., 1986, Nat 320, 595

Born M., Wolf E., 1980, Principle of Optics. Pergamon Press, Oxford

Bracewell R.N., 1986, The Fourier Transform and Its Applications. Mc Graw-Hill

Brault J., 1985, Fourier Transform Spectrometry. In: Benz A., Huber M., Mayor M. (eds.) High resolution in Astronomy. Geneva Observatory, Saas-Fee, p. 1

Colavita M.M., Shao M., Staelin D.H., 1987, Appl. Opt. 26, 4106

Conan J.M., Madec P.Y., Rousset G., 1992, 13th Sacramento Peak Summer Workshop on Real time and post-facto solar image correction

Coudé du Foresto V., Ridgway S.T., 1991. In: Beckers J., Merkle F. (eds.) High-resolution imaging by interferometry II. ESO, Garching, p. 731

Coudé du Foresto V., Ridgway S.T., Mariotti J.-M., 1992. In: Volonté S. (ed.) Targets for Space-Based Interferometry. ESA, Beaulieu, p. 219

Danchi W.C., Arthur A., Fulton R., et al., 1986, Proc. SPIE 628, 422

Davis J., Lawson P.R., Booth A.J., Tango W.J., Thorvaldson E.D., 1995, MNRAS (in press)

Feichtinger H.G., Gröchenig K., Strohmer T., 1995, Numerische Mathematik 69, 423

Jennison R.C., 1958, MNRAS 118, 276

Goodman J.W., 1985, Statistical Optics. John Wiley & Sons, New York

Itoh K., Ohtsuka Y., 1986, JOSA 3, 94

Mariotti J.-M., Ridgway S., 1988, A&A 195, 350

Mariotti J.-M., Coudé du Foresto V., Perrin G., Zhao Peiqian, Léna P., 1995, A&A (in press)

Perrin G., Coud e du Foresto V., Ridgway S.T., Mariotti J.-M., Benson J.A., 1995, proc. SPIE 2476, 120

Readhead A.C.S., Nakajima T.S., Pearson T.J., et al., 1988, AJ 95, 1278

Ridgway S.T., Joyce R.R., Connors D., Pipher J.L., Dainty C., 1986, ApJ 123, 1234

Rigaut F., Mariotti J.-M., 1995, A&A (in preparation)

Roddier F., 1981. In: Wolf E. (eds.) Progress in Optics Vol. XIX, 283

Shao M., Colavita M.M., Hines B.E., et al., 1988, A&A 193, 357

Shao M., 1992, ARA&A 30, 457